Calculation of Landé *g* factors for III-V nanowhisker quantum dots and comparison with experiment

A. De and Craig E. Pryor
Department of Physics and Astronomy and Optical Science and Technology Center, University of Iowa, Iowa City, Iowa 52242, USA
(Received 10 May 2007; revised manuscript received 9 August 2007; published 25 October 2007)

The coupling between a magnetic field and the spin of an electron confined to a quantum dot is determined by the *g* factor, which is strongly affected by the structure of the dot. Uncertainties in a dot's geometry and composition can obscure quantitative comparison of theory and experiment. Nanowhisker quantum dots (NWQDs) provide a well-controlled structure that is ideal for such comparison. We have performed detailed three-dimensional numerical calculations of the electronic properties of NWQDs consisting of an InP/InAs/InP quantum well embedded in a [111] oriented InAs nanowhisker. We have computed *g* factors, confinement energies, and wave functions for valence and conduction states as a function of dot size. The calculations are in excellent agreement with experiments and differ markedly from *g* factors obtained from extrapolation of bulk formulas, providing strong confirmation of the effect of angular momentum quenching. The closeness of our results to experiment enables us to identify critical well and barrier widths yielding $g \approx 0$, which are important for technological applications. We also predict larger and more negative *g* factors for $\vec{B}$ oriented along [111]. The calculations were carried out using eight-band strain-dependent $k \cdot p$ theory in the envelope-function approximation using a finite difference technique on a real-space grid.

DOI: 10.1103/PhysRevB.76.155321 PACS number(s): 73.21.La, 76.30.−v

I. INTRODUCTION

The effective magnetic moment of an electron confined to a semiconductor nanostructure is influenced by material properties, the confining potential, and strain. Recently, it was shown that confinement plays a pivotal role in the *g* factor of a carrier confined to a quantum dot,[1] significantly modifying the *g* factor from the value corresponding to the bulk materials from which the quantum dot is constructed. There have been measurements of *g* factors in a variety of quantum dot (QD) systems, including self-assembled quantum dots (SAQDs),[2,3] nanocrystals,[4] and dots formed from quantum well thickness fluctuations.[5] SAQDs provide the most challenges for comparing theory and experiment because of the experimental uncertainties in geometry and composition, but provide the richest physics due to the presence of strain and anisotropic geometry.

Recently, *g* factors have been measured in a new type of QD[6] grown using a chemical beam epitaxy bottom-up fabrication technique.[7–9] These QDs are especially interesting since they contain lattice mismatched materials, yet do not suffer from the uncertainties in geometry and composition which make comparison of theory and experiment difficult for SAQDs. The QDs are grown by embedding an InP/InAs/InP quantum well in a [111] grown InAs nanowhisker, resulting in quantum confinement between the InP barriers. These nanowhisker quantum dots (NWQDs) are characterized by their well-controlled growth, clean interfaces, and the absence of intermixing,[9] making them one of the few types of QDs for which the structural geometry is precisely known. Hence, these NWQDs are ideal for testing theoretical approaches to QD electronic structure.

We have calculated energies, wave functions, and *g* factors for electrons confined to NWQDs. Our results are in excellent agreement with the experimentally measured magnitudes of the *g* factors. We find that the calculated *g* is strongly dependent on the size of the NWQD and the thickness of the barriers, which is consistent with experiments. We have also calculated the sign of *g*, which is not experimentally determined in transport measurements.

II. METHODOLOGY

Figure 1 shows a typical NWQD in its measurement geometry, as described in Ref. 9. This structure consists of an InP/InAs/InP quantum well (QW) embedded in an InAs nanowhisker, oriented along the [111] direction. Unlike self-

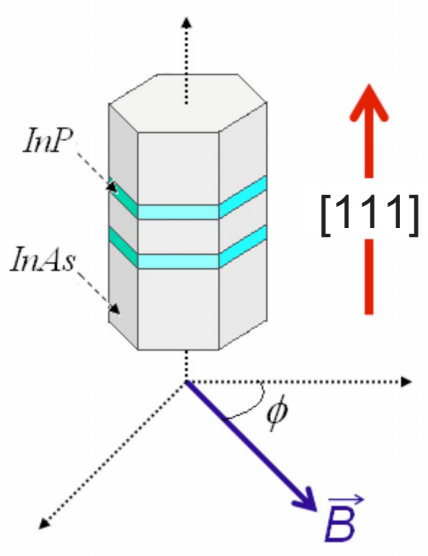

FIG. 1. (Color online) Schematic of a typical nanowhisker QD used in *g* factor measurements. $\vec{B}$ is the magnetic field and ϕ is the azimuthal angle of $\vec{B}$.

assembled QDs, the structure consists of pure InAs and InP with no intermixing. The growth conditions give rise to a wurtzite (WZ) crystal structure, resulting in the whisker having a hexagonal cross section. The applied magnetic field is perpendicular to the whisker's growth direction, but the azimuthal angle is arbitrary.

All calculations were done numerically using real-space $k \cdot p$ theory[10] with an eight-band strain-dependent model.[11,12] The strain was calculated using continuum elasticity theory and finite elements. Material parameters were taken from Ref. 13 assuming temperature $T=0$. The cubic real-space grid was oriented along the directions corresponding to the cubic crystal symmetry with the [111] whisker along the body diagonal of the cubic computational box. This necessitated a large 250^3-site grid for the strain calculation, which was then truncated to just fit the well and barrier for the electronic calculations. g factors were found by calculating the Zeeman splitting in a uniform magnetic field B using the Hamiltonian described in Ref. 1. The g factor was then determined by $g=\Delta E/\mu_B B$, where μ_B is the Bohr magneton.

Although the NWQDs have WZ structure, a zinc-blende (ZB) Hamiltonian was used since WZ material parameters for InAs are not known. For direct-gap III-V semiconductors, it has been shown that WZ and ZB materials have band gaps differing only slightly,[14,15] and the dispersion of WZ materials at the Γ point is well approximated by assuming a ZB structure.[16] As a check, we also performed calculations using a ZB Hamiltonian with energy gaps modified to match estimated WZ values.

The coupling of the whisker to the QD presents a technical problem since there is no true bound state in the QD. In order to ensure that QD states were calculated rather than states in the whisker lead, the band-edge energies in the whisker were artificially changed to match the InP barrier. This only affected the electronic calculations as the strain was computed using unmodified material parameters. This technique raised the computed energies slightly due to the additional confinement, but by varying the amount by which the InAs energy was shifted, we estimated the change in confinement energy to be on the order of only a few meV. The effects of tunneling into the whisker lead are illustrated in Fig. 2, where the wave functions are shown with and without the modification of the whisker material.

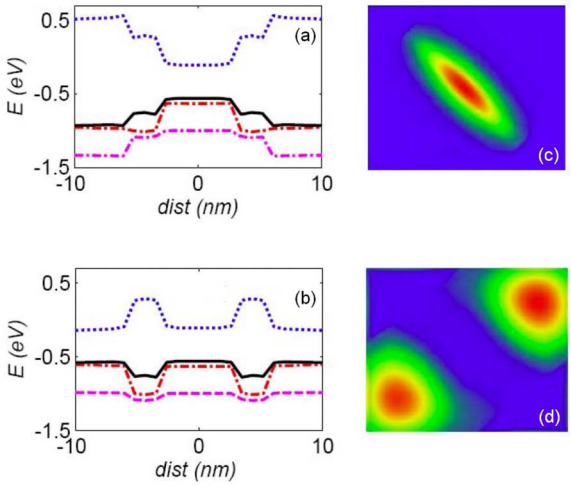

FIG. 2. (Color online) (a) NWQD zone center band structure with artificially raised InAs barrier. (b) InAs barrier with regular band parameters. (c) Electronic wave function corresponding to (a), contained with the NWQD. (d) Electronic wave function corresponding to (b), tunneling out into the whisker.

III. RESULTS

A. Nonlinearities and anisotropies

Due to the large size and small confinement energy of a NWQD, a nonlinear dependence of g on $\vec{B}$ should occur at a smaller field than in a strongly confined QD. To rule out significant nonlinearities in NWQDs, we calculated $g=\Delta E/\mu_B B$ as a function of magnetic field up to 4 T for various QD geometries. We found that the nonlinearities were insignificant ($<0.1\%$) over this range of fields, and for all subsequent calculations, $B=1$ T was used.

Another potential complication in interpreting the experiments of Ref. 6 is the direction of the magnetic field. In the experiments, $\vec{B}$ was perpendicular to the whisker, while the azimuthal angle was random. In order to determine the importance of this randomness in interpreting the measurements, we calculated the g factor as a function of $\vec{B}$ field direction, ϕ. Since the azimuthal dependence of g was found to be negligible ($<0.4\%$), all subsequent calculations were done with $\vec{B}$ in the $[1\bar{1}0]$ direction.

B. Zinc-blende calculations

We first examine the dependence of the electron g factors on the NWQD diameter, D. Figure 3 shows the calculated g factors as a function of D for different InP barrier thicknesses and InAs well widths. As can be seen, g depends only very weakly on D, varying by less than 10% for 40 nm $\leq D \leq 70$ nm. We attribute this to the well widths being substantially smaller than the lateral cross section and, therefore, providing the dominant contribution to the confinement energy. Because the variation with D is so small, in the calculations that follow, we only consider $D=53$ nm.

Our main results are in Fig. 4, which shows calculated g factors as a function of the well and barrier widths, the experimental values from Ref. 6, and g factors calculated by approximating the QD as a bulk semiconductor with a modified band gap. The effects of confinement are clearly visible as decreasing well width and increasing barrier width both drive g from the bulk InAs value of $g=-14.4$ toward $g=2$. For a well width $w_{\mathrm{InAs}}<3$ nm, the effect is sufficient to make $g>0$. The calculated values are in excellent agreement with the experimental ones for a variety of geometries, though at smaller well widths ($w_{\mathrm{InAs}}<12$ nm) the calculated values lie just outside the experimental error bars.

While the eight-band $k \cdot p$ values show a small discrepancy with experiment, the g factors calculated using the bulk approximation are in complete disagreement with experiment. In a cubic semiconductor, the bulk electron g factor in

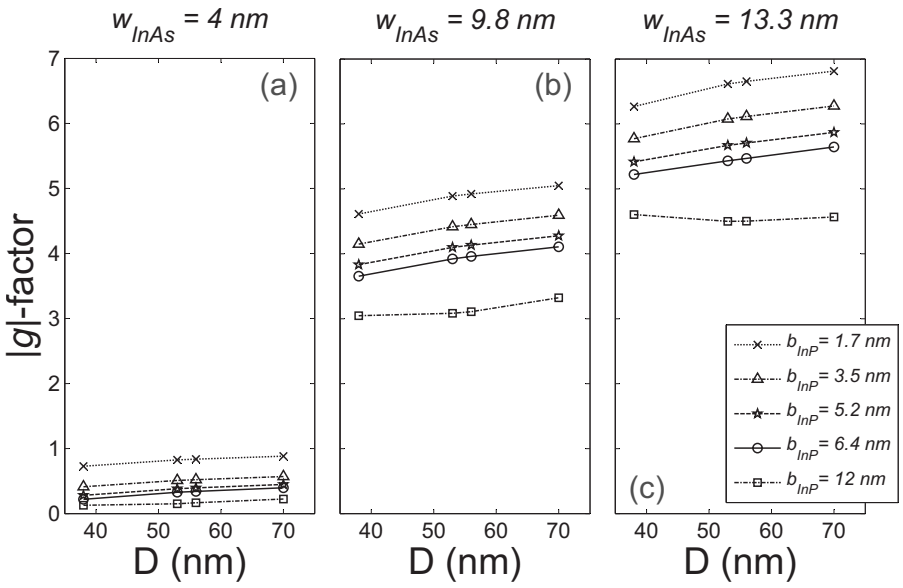

FIG. 3. g as a function of whisker diameter D for various InP barrier widths b_{InP} and for InAs well widths w_{InAs} of (a) 4 nm, (b) 9.8 nm, and (c) 13.3 nm.

the eight-band approximation is given by[17,18]

$$g = 2 - \frac{2E_P\Delta_{\mathrm{SO}}}{3E_g(E_g + \Delta_{\mathrm{SO}})}, \tag{1}$$

where E_g is the band gap, Δ_{SO} is the spin-orbit (SO) coupling, and $E_P = 2\langle S|P|X\rangle^2/m$ is the Kane matrix element involving s-like and p-like Bloch functions $|S\rangle$ and $|X\rangle$, respectively.[19] This expression may be applied to a QD by using the values of E_g and Δ_{SO} computed for the QD. The lower group of curves in Fig. 4 was obtained in this manner from Eq. (1), with E_g taken from a full calculation including the confinement energy and Δ_{SO} taken from the $k=0$ band energies including strain but not confinement. Application of the bulk approximation gives the correct trend as confinement drives g toward 2; however, the approximation severely underestimates the effects of confinement. The bulk approximation is in better agreement for large QDs, although g approaches the bare electron value too slowly with decreasing well width and yields the wrong sign for the smallest QDs. In contrast, the numerical calculations predict that g should rapidly approach the bare electron value as the size of the QD gets smaller due to angular momentum quenching in QDs.[1] Note that this will occur up until the critical limit, beyond which the excited bound states get squeezed out of the dot. The g factor would then approach that of the whisker, since the states with which the QD ground state mixes increasingly lie in the whisker.

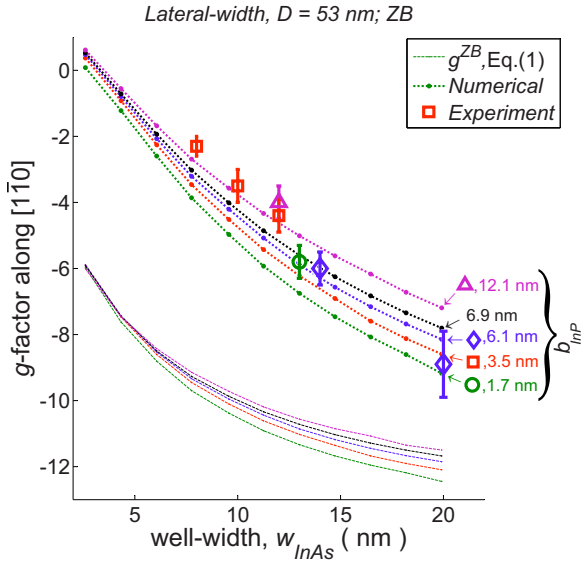

FIG. 4. (Color online) NWQD g factors versus well and barrier widths calculated using a ZB Hamiltonian and material parameters (Ref. 13). The upper set of curves are explicit numerical calculations, while the lower set of curves were calculated by extrapolating the bulk formula for ZB given by Eq. (1). The experimental points are measurements from Ref. 6. The energy gaps used for the bulk approximation were taken from the full electronic calculations, while the spin-orbit energies were taken to be that of the bulk material with the same average strain as that of InAs of the NWQD.

C. Quantum dot–whisker coupling

Figure 4 shows a small discrepancy between the calculated g and some of the experimentally determined values, particularly for thin InP barrier widths. As discussed in Sec. II, in order to confine the electronic wave function to the QD, the calculations were done by raising (lowering) the conduction (valence) band edge of the surrounding InAs whisker to match that of the InP barrier.

In order to estimate the coupling between the QD and the nanowhisker, we calculated transmission coefficients, through the NWQD structure, using a one-dimensional effective mass model. The results are shown in Fig. 5, where the transmission coefficients are plotted as a function of energy for well widths of 12 nm and barrier widths of 3.5 and 12 nm. As seen in Fig. 5, the width of the lowest resonance peak for the 3.5 nm barrier is about 2 orders of magnitude larger than the lowest resonance width for the 12 nm barrier. However, even for the 3.5 nm barrier, the resonance width is much smaller than the conduction band barrier height and,

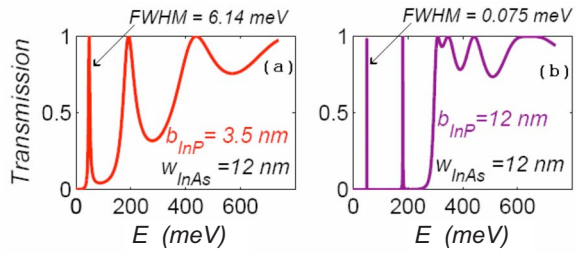

FIG. 5. (Color online) Plane wave transmission through a NWQD plotted as a function of energy for InAs well widths of 12 nm and InP barrier widths of (a) 3.5 nm and (b) 12 nm. Note that these correspond to two experimental points in Fig. 4 with $w_{\mathrm{InAs}}=12$ nm.

therefore, the QD is only weakly coupled to the whisker. Moreover, if the overall discrepancy between calculated g and experiment were largely due to the QD-whisker coupling, the experimentally measured g would tend to be closer to the bulk value. However, the opposite trend is seen between our calculations and measured g, as shown in Fig. 4. This suggests the presence of an additional unaccounted confinement mechanism in the NWQDs, which drives the experimental g factors toward the bare electron value.

D. Wurtzite corrections

Additional confinement is most likely to arise from the WZ structure of the NWQDs. It has been suggested by Murayama and Nakayama[15] that the zone center band gaps of WZ InAs and InP are slightly larger than their respective ZB counterparts. Following Ref. 15, we repeated the calculations after incrementing the band gap of InAs by 10% and that of InP by 6%. This raises the NWQD conduction band barrier height by about 50 meV, generating greater confinement for the electronic states. The strain causes a net increase in the barrier height even though the unstrained InP band gap is increased more than that of the InAs. The WZ band-gap energies were used with the ZB $k\cdot p$ Hamiltonian, which is a good approximation in the vicinity of the Γ point for WZ,[16] as noted earlier.

The results using WZ band gaps are plotted in Fig. 6, along with experimental results and g obtained from the bulk approximation. Using WZ band gaps improves the agreement with experiment, and the results for 1.7, 6.1, and 12.1 nm barriers are all within the experimental error bars. The result for a 12.1 nm barrier is in exceptionally good agreement as is expected, since our technique of using completely confined wave functions best suits the NWQDs with the thickest barrier. For a 3.5 nm barrier, the value of g calculated with WZ gaps lies outside the error bars, but is in better agreement than the value using ZB parameters (Fig. 4). For $w_{\mathrm{InAs}}\approx 20$ nm and InP barrier widths $b_{\mathrm{InP}}\approx 6$ nm, the ZB result is in better agreement with experiment than the value with WZ gaps, however, the error bars on the experimental value are also quite large. The difference between g calculated using ZB and WZ parameters is shown in Fig. 7. As can be seen, the overall difference between the calculations using ZB and WZ parameters is largest for small well

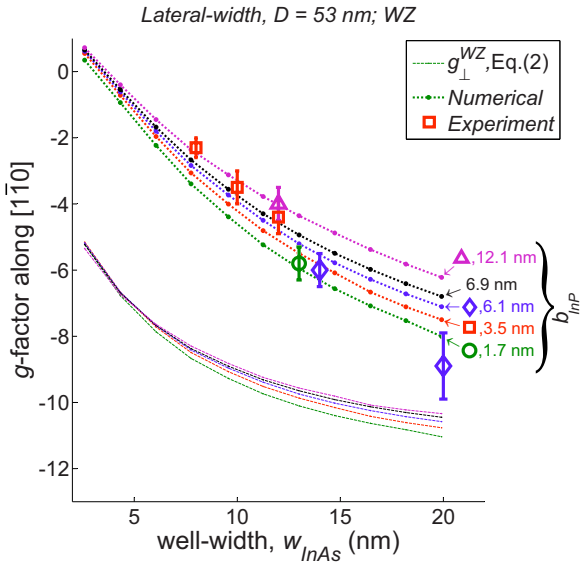

FIG. 6. (Color online) NWQD g factors versus well and barrier widths calculated using a ZB Hamiltonian and estimated WZ material parameters. The WZ parameters were estimated by increasing the gaps of InAs and InP by 10% and 6%, respectively (Ref. 15). The upper set of curves are explicit numerical calculations, while the lower set was calculated by extrapolating the bulk formula for WZ given by Eq. (2). The value of q_7 was taken from Refs. 16 and 20. The energy gaps used with the bulk approximation were taken from the full electronic calculations, while the spin-orbit energies were taken to be that of the bulk material with the same average strain as that of InAs of the NWQD.

widths (which also have $g>0$) and small barrier widths.

Note that in Fig. 6 the bulk approximation is based on the g factor for a WZ crystal, given by[18]

$$g_{\perp}=2-\frac{E_P}{2}\left(\frac{1}{E_c-E_{so}}-\frac{1}{E_c-E_{lh}}\right)[2q_7^2(1-q_7^2)]^{1/2}, \quad (2)$$

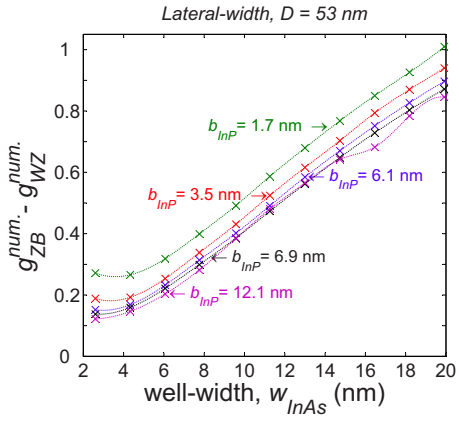

FIG. 7. (Color online) Difference between g factors calculated assuming a ZB structure and those obtained using WZ band gaps in the ZB Hamiltonian. The dotted lines are a guide for the eye.

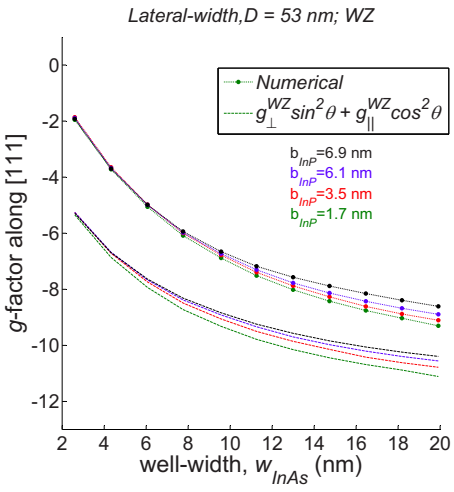

FIG. 8. (Color online) Calculated g factors for $\vec{B}$ oriented along the [111] growth direction. The numerically evaluated g factors are compared to those obtained for bulk WZ along [111]. For calculating g factors using the WZ bulk formula, we used confinement energies and strain-dependent band-edge energies for each individual structure.

$$g_{\parallel} = 2 - \frac{E_P}{2}\left(\frac{q_7^2}{E_c - E_{so}} + \frac{1 - q_7^2}{E_c - E_{lh}} - \frac{1}{E_c - E_{hh}}\right), \qquad (3)$$

where the anisotropic g factors are $g_x = g_y = g_{\perp}$ and $g_z = g_{\parallel}$, E_j is the energy at the jth band edge with indices c, lh, hh, and so corresponding to conduction, heavy hole, light hole, and split off, respectively, and $q_7^2 = E_{so}/(E_{lh} + E_{so})$ is a coupling that mixes spin-up and spin-down conduction states with the valence states.[16,20] The confinement energies were included in E_c, while the hh, lh, and so band-edge energies were obtained as the $k=0$ energies including the effects of strain but not confinement.

E. Predictions

We have also calculated g factors for $\vec{B}$ oriented along the [111] growth direction. These are shown in Fig. 8, along with g factors estimated in the bulk approximation

$$g_{eff} = g_{\perp} \sin^2 \theta + g_{\parallel} \cos^2 \theta, \qquad (4)$$

where θ is the polar angle between the z axis and the growth direction. Two striking features are that the variation with barrier thickness is smaller and the values of g are more negative for $\vec{B}$ along [111] than for perpendicular $\vec{B}$. In particular, for the smallest well width, perpendicular $\vec{B}$ gives $g > 0$, while $g \approx -2$ for $\vec{B}$ along [111].

Notice that in Fig. 8, the g factors along [111] have a decreasing dependence on the InP barrier width as the InAs well width gets smaller. For well widths less than 5 nm, there appears to be no noticeable variation in g with barrier width. Similar trends are seen in the bulk approximation using Eq. (4), although quantitatively the results are very different.

The magnetotransport measurements done in Ref. 6 did not determine the sign of g. Based on our calculated wave functions, we find that g is negative for all the measurements in Ref. 6. The signs were determined by examining the spin directions of the spin-split eigenstates. In general, it is obvious that the measured g factors should be negative as they all have magnitudes greater than 2. We find that $g < 0$ for all the NWQDs except the smallest structures. As seen in Fig. 6, the critical InAs well width for which $g \to 0$ is dependent on the InP barrier width.

Structures with $g \approx 0$ have been theoretically studied previously.[21] The critical well and barrier widths yielding $g \approx 0$ in NWQDs are important for several technological applications. For example, an entanglement preserving photodetector,[22] which converts photon polarization to electron spin, should also be engineered for $g \approx 0$, as the detector's up and down spins must respond equally to oppositely polarized photons. Engineering QDs with $g \approx 0$ may also facilitate optimal electric field control of g factors. Spin manipulation using electric field modulation of the electronic g factors has already been demonstrated in QWs.[23,24] Thus, essential quantum computing processes, such as ultrafast spin manipulation and single-qubit gate operations,[25] can be realized by externally driving spin resonance in a static magnetic field.

IV. SUMMARY

We have calculated confinement energies, wave functions, and g factors for ground state electrons in [111] oriented NWQDs, considering $\vec{B}$ oriented both along the nanowire and perpendicular to it. We predict that g is larger and more negative for $\vec{B}$ along [111]. We find excellent quantitative agreement between calculated g and experimentally measured values over a wide range of NWQD sizes. Our calculations give a negative g factor for all the experimentally measured structures, but we find a crossover to $g > 0$ for smaller NWQDs. Because $g \approx 0$, these structures are promising for g tensor modulation, which would benefit from large fractional changes in g.

ACKNOWLEDGMENTS

We wish to thank Lars Samuelson and Andreas Fuhrer for helpful conversations. This work was supported by funds from the University of Iowa.

[1] C. E. Pryor and M. E. Flatté, Phys. Rev. Lett. **96**, 026804 (2006).
[2] G. Medeiros-Ribeiro, M. V. B. Pinheiro, V. L. Pimentel, and E. Marega, Appl. Phys. Lett. **80**, 4229 (2002).
[3] G. Medeiros-Ribeiro, E. Ribeiro, and H. Westfahl, Jr., Appl. Phys. A: Mater. Sci. Process. **77**, 725 (2003).
[4] M. Bayer, A. Kuther, A. Forchel, A. Gorbunov, V. B. Timofeev, F. Schäfer, J. P. Reithmaier, T. L. Reinecke, and S. N. Walck, Phys. Rev. Lett. **82**, 1748 (1999).
[5] A. R. Goñi, H. Born, R. Heitz, A. Hoffman, C. Thomsen, F. Heinrichsdorff, and D. Bimberg, Jpn. J. Appl. Phys., Part 1 **39**, 3907 (2000).
[6] M. T. Bjõrk, A. Fuhrer, A. E. Hansen, M. W. Larsson, L. E. Froberg, and L. Samuelson, Phys. Rev. B **72**, 201307 (2005).
[7] M. T. Björk, B. J. Ohlsson, T. Sass, A. I. Persson, C. Thelander, M. H. Magnusson, K. Deppert, L. R. Wallenberg, and L. Samuelson, Nano Lett. **2**, 87 (2002).
[8] M. T. Björk, B. J. Ohlsson, C. Thelander, A. I. Persson, K. Deppert, L. R. Wallenberg, and L. Samuelson, Appl. Phys. Lett. **81**, 4458 (2002).
[9] N. Panev, A. I. Persson, N. Sküld, and L. Samuelson, Appl. Phys. Lett. **83**, 2238 (2003).
[10] C. Pryor, Phys. Rev. B **44**, 12912 (1991).
[11] C. Pryor, M.-E. Pistol, and L. Samuelson, Phys. Rev. B **56**, 10404 (1997).
[12] C. Pryor, Phys. Rev. B **57**, 7190 (1998).
[13] I. Vurgaftman, J. R. Meyer, and L. R. Ram-Mohan, J. Appl. Phys. **89**, 5815 (2001).
[14] C. Y. Yeh, S. H. Wei, and A. Zunger, Phys. Rev. B **50**, 2715 (1994).
[15] M. Murayama and T. Nakayama, Phys. Rev. B **49**, 4710 (1994).
[16] S. L. Chuang and C. S. Chang, Phys. Rev. B **54**, 2491 (1996).
[17] S. Zwerdling, B. Lax, L. M. Roth, and K. J. Button, Phys. Rev. **114**, 80 (1959); L. M. Roth, B. Lax, and S. Zwerdling, *ibid.* **114**, 90 (1959).
[18] C. Hermann and C. Weisbuch, Phys. Rev. B **15**, 823 (1977).
[19] E. L. Ivchenko and G. E. Pikus, *Superlattices and Other Heterostructures* (Springer, New York, 1997).
[20] M. W. Bayerl, M. S. Brandt, T. Graf, O. Ambacher, J. A. Majewski, M. Stutzmann, D. J. As, and K. Lischka, Phys. Rev. B **63**, 165204 (2001).
[21] A. A. Kiselev, E. L. Ivchenko, and U. Rössler, Phys. Rev. B **58**, 16353 (1998).
[22] H. Kosaka, A. A. Kiselev, F. A. Baron, K. W. Kim, and E. Yablonovitch, Electron. Lett. **37**, 464 (2001).
[23] Y. Kato, R. C. Myers, D. Driscol, A. C. Gossard, J. Levy, and D. D. Awschalom, Science **299**, 1201 (2003).
[24] G. Salis, Y. Kato, K. Ensslin, D. C. Driscoll, A. C. Gossard, J. Levy, and D. D. Awschalom, Nature (London) **414**, 619 (2001).
[25] D. Loss and D. P. DiVincenzo, Phys. Rev. A **57**, 120 (1998).